Automatic Spinal Canal Breach Detection During Pedicle Screw Placement

L. Leblanc, E. Saghbini, J. Da Silva, A. Harlé, S. Vafadar, T. Chandanson, R. Vialle, G. Morel, Brahim Tamadazte

Automatic Spinal Canal Breach Detection During Pedicle Screw Placement

L. Leblanc[1], E. Saghbini[1,3], J. Da Silva[1,2], A. Harlé[1], S. Vafadar[1], T. Chandanson[2]
R. Vialle[3], G. Morel[1], and B. Tamadazte[1] .

***Abstract*— Precise pedicle screw placement is imperative for a range of spinal procedures, demanding exact geometric alignment while also carrying inherent risks. The literature reports a complication rate in the case of screw mispositioning of up to 18%. To increase the accuracy of pedicle screw placement, we developed a robotic setup and a breach detection algorithm that could detect a possible perforation of the spinal canal. The robotic setup includes a robotic arm, a drilling system, and specific sensors, e.g., electrical conductivity at the drill bit's tip. The breach detection algorithm consists of a Bayesian-based method providing online and real-time analysis of the electrical conductivity signal to predict a breach. The robotic setup and the perforation detection algorithm were assessed in two ex-vivo experiments. First, data collection was performed by drilling 80 fresh pig vertebrae pedicles, followed by precise data labelling by a surgeon. The evaluation of the proposed algorithm was conducted numerically. Finally, the assessment was performed online by automatically drilling into pedicles in conditions similar to the operating room. The results demonstrated that the algorithm could predict perforations and prevent the robotic setup from going through in 100% of 24 drilled vertebrae. Results demonstrate that using electrical conductivity combined with a robotic setup allows the detection of imminent perforations of the spinal canal during pedicle drilling. This was the first study to evaluate spinal canal perforation detection during ex-vivo pig pedicle drilling.**

I. INTRODUCTION

Pedicle screw (PS) placement in spine surgery has been considered a standard surgical procedure for the past forty years. It is widely used for various spinal procedures, especially in the case of spinal deformities, e.g., scoliosis [1]. Different forms of scoliosis can occur in both young and adult patients. Clinical grading of scoliosis is based on the severity of the angular deformity, measured by the Cobb angle [2], defined as the angle between the endplates of the most tilted vertebrae of the curve [3]. Scoliosis can be idiopathic, creating pathologies like neuromuscular disorders, malformations, and other syndromes [4]. It can cause muscular pain associated with a continuous effort to maintain the spine's balance or even neurological pain associated with narrowing the spinal canal. From 70° not 75° angulation onwards, there are repercussions on respiratory function [5].

This work has been supported by EU's H2020 research and innovation program under grant agreement No. 101016985 (FAROS. project)

[1]Authors are with Sorbonne Université, CNRS UMR 7222, INSERM U1150, ISIR, F-75005, Paris, France. leblanc@isir.upmc.fr

[2]Author is with SpineGuard SA, 10 cours Louis Lumière, 94300 Vincennes, France

[3]Authors are with Sorbonne Université, Groupe de Recherche Clinique "Robotique et Innovations Chirurgicales" (GRC33), Hôpital Armand-Trousseau 26 Ave du Docteur Arnold Netter, 75012 Paris, France.

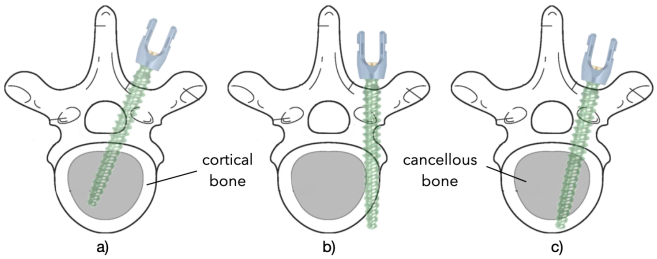

Fig. 1. Different scenarios for screw insertion into the vertebrae: a) leading to a medial perforation (i.e. spinal canal perforation), b) leading to a lateral perforation and c) well-placed screw.

Scoliosis treatment depends on the angular deformity's aetiology and severity. In young patients, the risk of evolution and angulation determines the treatment. For instance, when the deformation is below 20°, the patient will typically require only regular monitoring. For curves between 20° and 50°, the patient is treated with a brace to limit the progression of the disease. However, surgical intervention is usually indicated for more severe deformities, i.e., those greater than 50°. The surgical treatment, also known as *arthrodesis*, consists of spinal fusion by implantation of PS and rods [6]. The PS should be positioned correctly to obtain maximum stability of the bone-screw interface while avoiding a perforation in the spinal canal during insertion (Fig. 1). This highlights that the success of spinal surgery depends substantially on the ability to position the PS safely and accurately [7].

Drilling the pedicles for screw positioning is a challenging procedure. Failure can lead to injuries to major vessels (aorta, vena cava) or the spinal cord [8]. The literature reports a complication rate in the case of screw mispositioning of up to 18% [9]. The screw insertion task is performed free-hand, with intraoperative X-ray control or navigation guidance. Patient-specific guides are used to increase accuracy [10]. In some cases, a passive robot is used to immobilize the screw trajectory at the entry point while allowing the surgeon to perform the drilling task [11]. However, the most established techniques are navigation systems combined with a preoperative registration phase and robotic solutions. A well-known technical limitation of these solutions is the loss of accuracy due to imaging [12] and registration errors [13], [14] in addition to the risk of radiation exposure resulting from X-ray imaging.

II. MOTIVATION AND CONTRIBUTIONS

Although navigation approaches have contributed to improving spine surgical procedures, they present several limitations, particularly in terms of usability and accuracy. Accuracy is reduced because of the patient's breathing movement. Furthermore, a slight change in the patient's position during the pedicle preparation is sufficient to introduce registration errors [12], [15].

One of the advantages of a robotic approach in PS placement, beyond the functional accuracy it provides, is safety. Indeed, the use of a robotic system during the drilling phase allows instantaneous reaction (e.g., stopping the drilling) in tens of milliseconds, compared with manual drilling performed by a surgeon who may be slower to react. This is particularly true in certain procedures (e.g., on adult patients), where the surgeon has to apply relatively great force to drill into the bone. Additionally, drilling parameters (rotation speed, applied force and torque, etc.) can be precisely defined and kept constant (or adapted to suit the patient) throughout the procedure contrary to a manual procedure.

In the remainder of the paper, we will demonstrate that the use of the robot combined with an automatic breach detection method enables drilling to be stopped very early, i.e., within the first milliseconds of a change in the electrical conductivity signal used in our algorithm. In this spirit, we have proposed a robotic platform for PS insertion equipped with specific sensors, including the electrical conductivity sensor (hereinafter referred to as DSG sensor) developed by SpineGuard SA [16], [17] and many other sensors (force, position, vibrations, etc.). We then investigate the use of signals recorded by the mentioned sensors to detect perforations early during pedicle drilling. Real-time perforation detection is performed using a Bayesian-based method to detect changes in the behavior of the DSG signal. The developed robotic setup and the perforation detection algorithm are extensively evaluated, numerically and experimentally, based on the *Gertzbein-Robbins* classification of PS placement errors [18]. According to this classification, grade "A" indicates no spinal canal perforation, grade "B" indicates less than 2 mm of perforation in the spinal canal, grade "C" indicates 2–4 mm spinal canal perforation and grade "D" indicates more than 4 mm of perforation. Higher grades are associated with a higher risk of neurological complications. Grades "A" and "B" are considered clinically satisfactory. This paper extrapolates the *Gertzbein and Robbins* classification scale to pedicle drilling since no screw insertion is performed.

The numerical validation is achieved using a database created by performing 80 drillings. The results obtained are promising. Regarding the detection rate, an imminent perforation point, which corresponds to a deformation of the periosteal tissue that occurs just before the actual perforation, was detected in 25% of the drilling signals. Perforation was detected less than 2 mm after the actual perforation point in the 75% remaining signals. In total, 100% of perforation alerts were raised in a zone corresponding to the grades "A" and "B" for pedicle drilling. Regarding accuracy, the perforation point was detected with an average error of 0.50 mm (standard deviation = 0.71 mm) over the 80 drilled lumbar vertebrae.

An experimental validation run completes these first results. Twenty-four (24) vertebrae are drilled. For all vertebrae, the drilling process was automatically stopped just before perforation, exhibiting a 100% success rate. The experimental results reinforce those obtained in simulation and fully meet the requirements of such a surgical procedure.

III. RELATED WORKS AND BACKGROUND

Bone drilling is a routine procedure in various surgical disciplines (orthopaedics, neurosurgery, traumatology). As discussed, the drilling task is a delicate and challenging procedure that requires accuracy and safety. Detecting a potential breach when drilling a bone has consequently become an active research field. Various sensors are used to measure the drilling progress (force, speed, position, etc.). Therefore, identifying a possible breach is equivalent to detecting an unexpected change in the measured signal. Promising methods have been proposed in the literature. For instance, Brett et *al.* [19] proposed an algorithm for stapedotomy based on detecting the simultaneous increase of torque and the decrease of the feed force during the drilling procedure. Another similar work suggested tracking the gradient of the force signal (after filtering) to detect unexpected variations in the signal, meaning that the drill is breaching a femur bone [20]. Lee et *al.* [21] proposed using the trend and a threshold on both the torque and feed rate on various bone types (e.g., scapula, skulls, and femurs). Although these methods are promising, qualitative and quantitative evaluations are not provided. More recently, Hu et *al.* [22] suggested using feature functions based on the measured force for different drill shapes. For this purpose, cattle vertebrae drilling signals are used to identify threshold values which are then used to stop the drilling when the force reaches the transitional zone from the cancellous tissue into the cortical tissue. This study performed six experimental drillings; however, only one drilling hole was evaluated, demonstrating that the drilling stopped automatically at 0.97 mm before the breach. Besides, monitoring the electrical current through the drill motor [23] was used to detect unexpected changes in the signal to identify a potential breach within the safety zone. However, no metric evaluation is reported on sample size, success rate, or detection accuracy. The use of audio signal has also been investigated for breach detection purposes [24] demonstrating that processing the audio signal allowed discriminating cortical and cancellous bone tissue by analyzing the power spectral density. It is reported that using audio signals provides an 88% success rate in finding potential breaches over 35 drillings performed in pig vertebrae. However, no information on accuracy is provided in this study.

Preliminary work on breach detection [25] shows that the DSG signal can provide very interesting results. The reported

breach detection algorithm was tested on 104 lamb vertebrae, giving a 100% success rate. However, the drilling was carried out in the spinous processes emerging perpendicularly into the canal, thereby avoiding the tangential breaches that can occur when the pedicles are drilled. Furthermore, the proposed breach detection algorithm includes signal filtering and calibration phases. This method uses several parameters which must be defined beforehand such as absolute and relative conductivity thresholds and the definition of the expected local conductivity gradient (thresholds). Furthermore, it also includes an online filtering phase (moving averaging) of the DSG signal, which may introduce a delay in breach detection.

The following section describes the proposed method, which consists of Bayesian distribution for online inference. This method does not require a filtering phase or calibration parameters.

IV. BREACH DETECTION METHODOLOGY

A suitable and effective perforation detection algorithm should identify meaningful changes in the trend of signals of interest, operate in real-time, be accurate, robust to measurement noise (regardless of the sensor type), and have minimal parameter tuning. The latter indicates that the surgeon should not need to perform complex parameterization before or during the surgical procedure, e.g., depending on the vertebral bone quality.

Probabilistic and recursive methods are suitable candidates for the accurate detection of an abrupt change in a time series. Such change occurs at so-called changepoints (CPs), i.e., time instants when the probability distribution of a time series changes. The Bayesian Online Change Point Detection (BOCPD) algorithm [26] is one of the most promising CP detection methods and has been demonstrated in different fields (e.g., finance and environment). It has been found to be one of the best-performing methods for offline and online CP detection [27], [28].

A. Bayesian Online Changepoint Detection

Let $\mathbf{x} = (x_1, x_2, ..., x_n)^\top$ denote the data samples observed over time. In the present work, $\mathbf{x}$ is univariate, but the method can be extended to multivariate cases. Let $x_{1:t}$ denote the data samples observed between the initial time instant 1 and time instant t. CPs occur at unknown time instants between the initial time instant $t = 1$ and final time instant $t = n$. These CPs divide $\mathbf{x}$ into production partitions [26]. For each partition ρ, it is assumed that the data samples within that partition are independent and identically distributed and sampled from some probability distribution $P(x_t|\eta_\rho)$, where the parameters η_ρ are also considered independent and identically distributed.

BOCPD relies on computing the probability distribution of an intermediate variable, the "run length", i.e., the time since the most recent CP occurred [26]. The run length at time instant t is denoted as r_t. Observing $r_t = 0$ indicates that a CP occurred at time instant t. Arbitrarily, the first data sample observed is considered an additional CP occurring at initial time instant $t = 1$, implying that $r_1 = 0$. Let x_t^r denote the subset of observations associated with the run r_t. Between two consecutive time instants, the run length can either be reset to 0 if a CP occurred or be incremented by 1 if no CP occurred:

$$r_t = \begin{cases} 0 & \text{if a CP occurred} \\ r_{t-1} + 1 & otherwise \end{cases} \tag{1}$$

An illustration is provided in Fig. 2. A hypothetical univariate signal $\mathbf{x}$ is plotted in Fig. 2.a. As long as no CP occurs, r_t is incremented as shown in Fig. 2.b where solid lines indicate that the run length grows at the next time instant. Significant changes in the distribution of $\mathbf{x}$ occur at time instant 4 and time instant 9. At these time instants, r_t resets to 0, as illustrated in Fig. 2.b, where the dotted lines indicate that the current run is truncated and the run length drops to 0.

Once a new observation x_t is observed, we determine whether the run length r_t is incremented or reset to 0. To this end, we compute the posterior probability distribution $P(r_t|x_{1:t})$. In other words, BOCPD aims at finding the run length r_t at every time instant that best matches the data $x_{1:t}$ observed so far. In Bayesian terms, for every time instant t, one wants to find $r_t = \arg\max_r P(r_t = r|x_{1:t})$ where:

$$P(r_t|x_{1:t}) = \frac{P(r_t, x_{1:t})}{P(x_{1:t})} \tag{2}$$

Since in (2) only the joint distribution over the run length and observed data $P(r_t, x_{1:t})$ depend on r_t, one can focus on this distribution and rewrite it recursively [26]:

$$P(r_t, x_{1:t}) = \sum_{r_{t-1}} P(r_t|r_{t-1})\, P(x_t|r_{t-1}, x_t^r)\, P(r_{t-1}, x_{1:t-1}) \tag{3}$$

Equation (3) exhibits that $P(r_t, x_{1:t})$ can be expressed as a function of $P(r_{t-1}, x_{1:t-1})$. This provides a recursive message-passing algorithm for the joint distribution over the current run length and the data, assuming two other factors are computed: the CP prior and the posterior predictive. Fig. 2.c illustrates this message-passing algorithm. In this plot, the circles represent run-length hypotheses. The lines between the circles show the recursive transfer of probability mass between consecutive time instants. A probability distribution is associated with each circle, i.e., run-length hypothesis. For each hypothesis, the probability distribution parameters are obtained by updating the initial parameters prior using every data sample observed since the beginning of the run.

B. Changepoint Prior

$P(r_t|r_{t-1})$ is the prior over r_t given r_{t-1}. This prior is non-zero at only two outcomes, since r_t only changes to 2 possible values, as shown in (1). This provides computational efficiency to the method and the prior simplifies to (4), where $\mathcal{H}$ is referred to as a hazard function.

$$P(r_t|r_{t-1}) = \begin{cases} \mathcal{H}(r_{t-1} + 1) & \text{if } r_t = 0 \\ 1 - \mathcal{H}(r_{t-1} + 1) & \text{if } r_t = r_{t-1} + 1 \\ 0 & otherwise \end{cases} \tag{4}$$

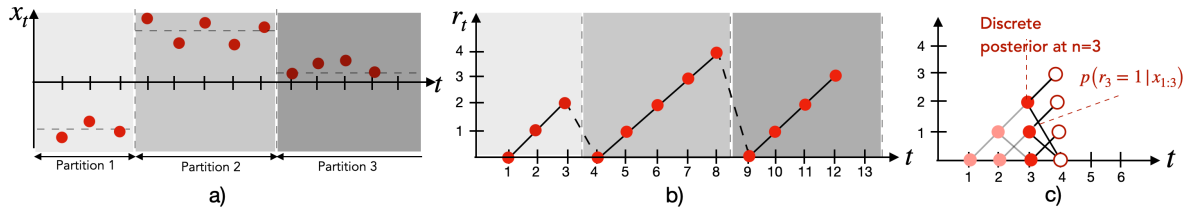

Fig. 2. Illustration of the BOCPD method for a) hypothetical univariate signal with distribution changes occurring at time instants $t = 4$ and $t = 9$. b) The most probable run length r_t drops to 0 when a changepoint is met. c) The trellis on which the passing algorithm lives: at each time instant, the probability of every run length is computed based on the data observed so far during the said run.

C. Posterior Predictive

$P(x_t|r_{t-1}, x_t^r)$ is the posterior predictive, i.e., the probability that the most recent datum belongs to a given run. Computing this posterior predictive can be challenging. Using conjugate exponential models can allow for more computational efficiency since they provide a closed-form expression of the posterior predictive. For instance, exponential families, which include many of the most common distributions, are good candidates and allow sequentially updating the distribution parameters as new data are observed [26].

D. Changepoint Detection

The original literature does not explicitly specify a determination criterion to declare a CP at a specific time instant [26]. Identifying a CP after a single sample of a new distribution may be challenging in certain cases, making it necessary to "wait" for N samples and evaluate the probability of a change happening N samples prior. Therefore, in terms of run length, detecting that r_t drops to 0 after a new observation is not an efficient criterion for accurate CP detection. Instead, we detect that r_t drops in a $[0, N]$ range.

E. Bayesian Online Perforation Detector

Building on the BOCPD approach, a Bayesian Online Perforation Detector is proposed. The overall functioning of the said detector is detailed in Algorithm 1. Regarding practical implementation, the following hypotheses are made:

1) A CP is declared if the run length drops in a $[0, 19]$ range.
2) $P(r_t|r_{t-1})$ is assumed to be constant both for simplicity and since no other prior information is available. Therefore, in Equation 4, $H(r_t) = \lambda^{-1}$, where λ is a parameter to adjust the algorithm sensitivity. A value of $\lambda = 250$ is empirically established.
3) As a generic assumption, normal distribution unknown mean and variance is assumed as a likelihood. The corresponding conjugate prior is a Normal-Inverse-Gamma distribution. The resulting posterior distribution is a generalized Student's T distribution with center μ_t, precision $\Lambda = \frac{\alpha_t \kappa_t}{\beta_t(\kappa_t+1)}$, and degree of freedom $2\alpha_t$ [29]:

$$P(x_t|r_{t-1}, x_t^r) = t_{2\alpha_t}(x_t|\mu_t, \frac{\beta_t(\kappa_t+1)}{\kappa_t \alpha_t}) \quad (5)$$

Parameters μ_t, κ_t, α_t, and β_t are initialized with pre-perforation distribution priors μ_0, κ_0, α_0, and β_0 at time instant $t = 0$. Then, at each time instant t, we want to model a new possible run of length 0, corresponding to the possibility of a CP. In this case, posterior predictive is computed using post-perforation distribution priors μ_{prior}, κ_{prior}, α_{prior}, and β_{prior}. These priors may be different from the initial values μ_0, κ_0, α_0, and β_0 to encompass the knowledge that a strong rise in the conductivity signal is expected upon perforation. The values of the distribution parameters priors used in the Bayesian Online Perforation Detector are provided in Table I.

TABLE I
DISTRIBUTION PARAMETERS PRIORS USED IN THE BAYESIAN ONLINE PERFORATION DETECTOR

Distribution parameter	Pre-perforation distribution	Post-perforation distribution
μ	$\mu_0 = 800$	$\mu_{prior} = 10000$
κ	$\kappa_0 = 1$	$\kappa_{prior} = 10$
α	$\alpha_0 = 10^{-6}$	$\alpha_{prior} = 10^{-6}$
β	$\beta_0 = 0.6$	$\beta_{prior} = 0.6$

At each time instant t, we also model the growth for already existing runs. This is achieved by computing the posterior predictive using parameters μ_t, κ_t, α_t and β_t for each run length value before updating these values with the latest datum observed:

$$\mu_{t+1} = \frac{\kappa_t \mu_t + x_{t+1}}{\kappa_{t+1}} \quad (6)$$

$$\kappa_{t+1} = \kappa_t + 1 \quad (7)$$

$$\alpha_{t+1} = \alpha_t + 0.5 \quad (8)$$

$$\beta_{t+1} = \beta_t + \frac{\kappa_t (x_t - \mu_t)^2}{2(\kappa_t + 1)} \quad (9)$$

V. DATA ACQUISITION SETUP AND PROTOCOL

To assess the proposed perforation detection algorithm, we conducted an ex-vivo experiment for data acquisition (to create a comprehensive database) and evaluated the proposed method. The experiments are done in conditions close to those of an operating room by drilling fresh pedicles and mimicking the physiological behaviour of the cerebrospinal fluid filling the spinal canal.

A. Drill bit and drilling system

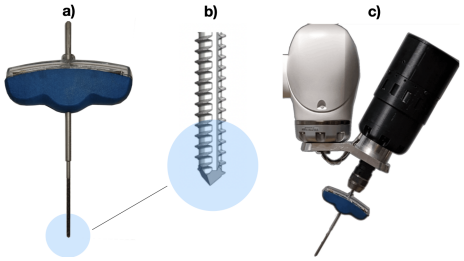

Fig. 3. a) Used drill bit equipped with an electrical conductivity sensor designed by SpineGuard SA, b) zoom on the "threaded" part of the drill and c) represent the drill bit mounted on the robotic arm.

The used drill bit is derived from instruments developed by SpineGuard SA (Fig. 3.a. It consists of a 3 mm diameter drill bit for cutting purposes with a pyramidal tip embedding a conductivity sensor and a threaded shaft (Fig. 3.b). The threaded shape of the drill continuously maintains the contact between the drill and the bone and avoids unwanted motion along the z-axis (i.e., the drilling axis). The drilling is carried out by a custom-made power drilling unit delivering 1.5 Nm nominal torque and a maximum speed of 922 rpm (revolutions per minute), able to perform drilling and screwing tasks. Finally, the drilling system is mounted on the robot's end-effector with an angle of 30° concerning the last robot axis (Fig. 3.c).

B. Robotic Setup and Embedded Sensors

The drilling system is rigidly fixed on a robotic arm, with an angle of 30°, as can be seen in Fig. 4. This robotic arm consists of a KUKA LBR Med 7 R800 robot adapted to medical requirements. It is equipped with built-in joint torque sensors allowing it to operate in a collaborative mode. It has a payload of 7 kg, featuring position accuracy of $\pm$0.15 mm and joint redundancy (7 degrees of freedom). The DSG sensor of the drilling system allows for distinguishing the different layers the drill bit passes through during the drilling process. The conductivity signal is low in the cortical layers compared to the one detected in the cancellous layers. However, the signal increases significantly once it intersects body fluid. Fig. 5 depicts an example of a typical DSG (proportional to the electrical conductivity) signal acquired by drilling a fresh pig vertebra. These tissue discrimination characteristics are suitable for detecting perforations (lateral or medial).

Algorithm 1 Bayesian Online Perforation Detector using the electrical conductivity signal

Input: x_t, DSG (electrical conductivity) signal in mV
Output: $Alert$, flag used to stop the drilling

Initialization: $P(r_1 = 0) \leftarrow 1$, $DetectionFlag \leftarrow False$,
for x_t **do**
  Calculate posterior predictive: $P(x_t|r_{t-1}, x_t^r)$
  Calculate growth probability: $P(r_t = r_{t-1}+1, x_{1:t}) = (1-\lambda_{prior}^{-1})P(x_t|r_{t-1}, x_t^r)P(r_{t-1}, x_{1:t-1})$
  Calculate changepoint probability: $P(r_t = 0, x_{1:t}) = \sum_{r_{t-1}} \lambda_{prior}^{-1} P(x_t|r_{t-1}, x_t^r)P(r_{t-1}, x_{1:t-1})$
  Calculate marginal probability: $P(x_{1:t}) = \sum_{r_t} P(r_t, x_{1:t})$
  Calculate run length distribution: $P(r_t|x_{1:t}) = P(r_t, x_{1:t})/P(x_{1:t})$
  Find $r_t = \arg\max_r P(r_t = r|x_{1:t})$
  Check that run length has exceeded the detection threshold once:
  if $r_t > threshold$ **then**
    $DetectionFlag \leftarrow True$
  end if
  Evaluate whether a change occurred:
  if $DetectionFlag$ & $r_t < threshold$ **then**
    $Alert \leftarrow True$
  end if
  Update distribution parameters
end for

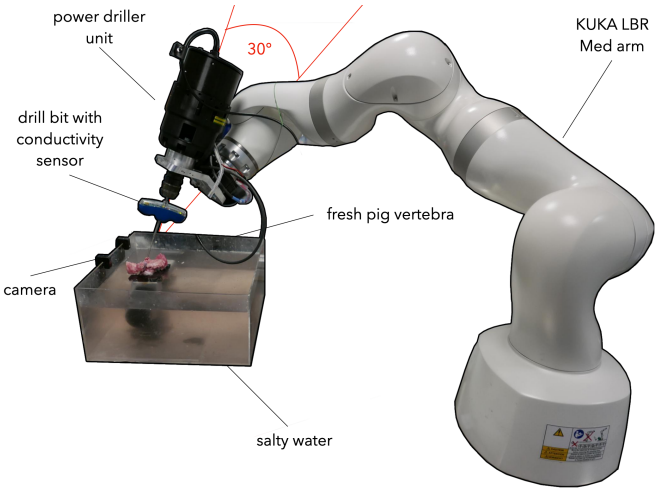

Fig. 4. Photography of the developed robotic set-up for spine surgery.

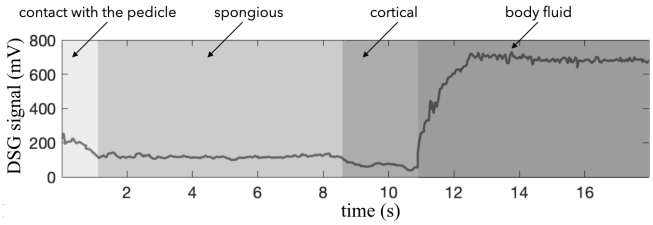

Fig. 5. An example of DSG signal acquired during a vertebra drilling process.

Although only the conductivity signal is used in the perforation detection algorithm, different signals issued from various embedded sensors (torque, position, velocity, time, video, etc.) are recorded and added to the database.

C. Drilling Workflow

We designed a drilling box where the vertebra (Fig. 6.a) is rigidly fixed in the drilling box. To simulate experimental conditions close to actual pedicle drilling in the operating room, the vertebra is submerged in a saline solution that approximately reproduces the electrical conductivity of cerebrospinal liquid contained in the spinal canal (Fig. 6.b). The saline solution is obtained by mixing 7g of salt per litre of tap water at a temperature in a [19.7, 24.6]° C range.

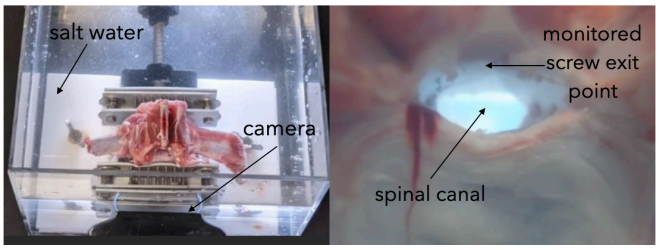

Fig. 6. Illustration of the data acquisition workflow: a) fixing the vertebra in salty water for drilling, and b) view of the frontal camera monitoring the drilling progress.

A camera is placed in front of the spinal canal to record the whole drilling procedure (Fig. 6.c).

D. Vertebrae Collection and Data Acquisition

To assess the developed methods and material, we collected fresh pig lumbar vertebrae from the butcher (Fig. 6.a). The fresh vertebrae were collected one day before the lab experiments and placed only in a refrigerator (since a freezer could have changed the properties of the bones or soft tissues).

For each drill, the surgeon collaboratively manipulated the robot to place the drill bit at the desired entry point and voluntarily aim for the spinal canal. They then adapted the contact force and drilling rotational speed according to the bone quality of the vertebrae. The force controller was developed earlier in another study [30]. Principally, the required force for drilling was empirically determined and set to f_d = 25 N. However, based on the bone's mechanical properties, the force f_d could reach up to 100 N. The drilling rotational speed was set at 60 rpm for all the performed drillings.

We recorded several additional signals such as torque, position (depth penetration of the drill bit), velocity, and time. Moreover, the camera filmed the spinal canal and captured the exact instant when the drill perforated into the canal.

A posteriori, three people independently watched the recorded video to identify the perforation time to avoid potential bias. The surgeon then labelled the exact time instant the perforation started. This allowed us to label all the other signals to build the database (see range highlighted in green in Fig. 7). This provides the ground truth for further assessment of the proposed perforation detection algorithms.

In total, 80 lumbar vertebrae were drilled.

VI. NUMERICAL AND EXPERIMENTAL VALIDATIONS

The first evaluation of the proposed perforation detection algorithm was carried out on the collected data. Hence, we evaluated offline the electrical conductivity signals recorded for each drilling (80 in total). Note that for each signal, the surgeon defined the exact time instant of perforation by *a posteriori* visualizing the videos recorded during the drilling. This task allows grading perforation detection according to our derivation of the *Gertzbein-Robbins* classification [18]. Detecting an imminent perforation before the actual point of perforation corresponds to grade "A," while declaring a perforation less than 2 mm after the actual perforation point corresponds to grade "B." In other words, the detection is considered acceptable if a perforation alert is raised before the right-most limit blue line of the green area in Fig. 7.

A. Numerical Validation

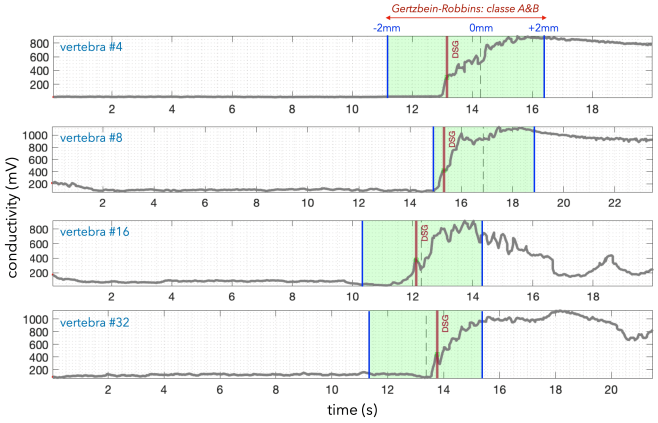

Fig. 7. Four examples of detected perforations (see vertical red lines) on the recorded DSG signals. A $\pm$2 mm green zone (delimited by the vertical blue lines) centred on the perforation instant (dotted lines) is plotted for visualization. Detection must occur before the upper limit of the green zone to be considered satisfactory (i.e. grade "*A*" or "*B*" perforations).

For the 80 drilled vertebrae, the success rate of the perforation detection is 100% meaning that the perforation was detected before it actually occurred or just at the instant of deformation of the periostal tissue (inner surface covering the spinal cord). From a clinical point of view, this corresponds to grades "A" and "B" according to the *Gertzbein-Robbins* classification [18]. In detail, 25% of the drillings are classified as "A" (imminent perforation is detected before the actual perforation point) and 75% as "B".

In terms of accuracy, our algorithm allows stopping the drilling with an average error (i.e., distance from the perforation point) of 0.50 mm with a standard deviation (STD) of 0.71 mm.

Figure 7 shows some examples of electrical conductivity signals for which the perforation is detected. As can be seen, the detection of the perforation (red lines shown in Fig. 7) corresponding to the abrupt change in the signal can occur before or slightly after the perforation point. Variability in the electrical conductivity signals can lead to detection after the perforation point, but always less than 2 mm after said point. The perforation detection over the whole set of the 80 performed drilling is summarized in Fig. 8, where Fig. 8.a depicts the distance of the automatic stop to the perforation point for each drilled vertebra, and Fig. 8.b shows the histogram of all the computed distances.

B. Experimental Results

We experimentally assessed the robotic setup and the perforation detection algorithm based on the numerical eval-

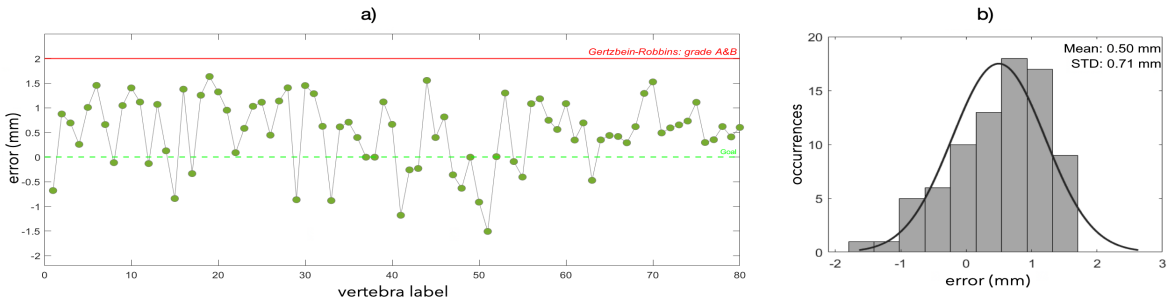

Fig. 8. Qualitative analysis over the 80 performed drillings. a) distance of the automatic stop to the bone interface for each drilled vertebra according to our derivation of the *Gertzbein-Robbins* classification (the boundaries of the "A" and "B" grades are represented by a red line) and b) the histogram of the resulting computed distances over the 80 drilled vertebrae.

uation and obtained promising results regarding accuracy and safety during the drilling procedure.

The experimental procedure is identical to the one used to build our database. For this purpose, we used another group of fresh vertebrae. The surgeon moved the drill bit to the entry point of the pedicle (by manipulating the robotic arm), and the drilling was automatically performed. The robot drilled 24 fresh lumbar pig vertebrae. The perforation detection algorithm stopped the drilling online automatically (without any calibration or pre-setting procedure compared to the numerical validation procedure (Section VI-A)). Once the vertebrae were drilled, the surgeon cut the pedicles along the drilled hole to verify where the drilling stopped. After investigation, it was shown that for all 24 drilled vertebrae, the drilling process was automatically stopped just before the perforation, i.e., exhibiting a 100% success rate.

Figure 9.a shows an example of an automatic stop of a drilling task before the perforation on the spinal canal with a safety margin of approximately 1 mm (Fig. 9.b).

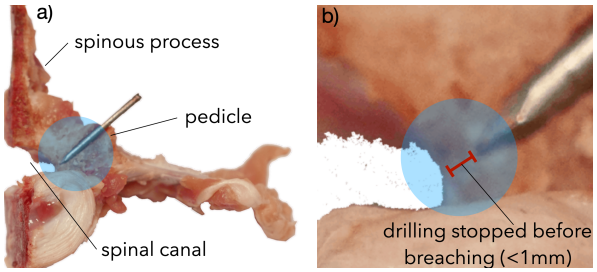

Fig. 9. Illustration of an automatic stop of a drilling process before perforation.

Figure 10 depicts a sample of 5 (among a total of 24) drilled vertebrae after cutting the pedicles along the drilled holes. Fig. 10.a shows a global view of the 5 vertebrae and Fig. 10.b shows the corresponding zoom on the drilled holes, while Fig. 10.c depicts the CT-scan images realized retrospectively. It can be seen on the CT-scan images that the proposed algorithm, coupled with the robotic platform, makes it possible to stop just at the moment of deformation of the periostal tissue covering the inside of the spinal canal. This means that although the detection error of the perforation is within a [0, +2] mm range according to our metric, this does not necessarily indicate an actual perforation in the canal. The retrospective inspection (CT scan) of the 24 vertebrae drilled under real conditions also showed a 100% success rate in avoiding a breach in the canal.

Furthermore, the robotic platform and the breach detection method were evaluated in another context, i.e. drilling a fresh sheep skull. It was shown that breaches were avoided (several drillings were carried out) without any change to the algorithm parameters or any further calibration phase being required.

VII. CONCLUSION

Spinal canal perforation can be associated with screw instability and neurological complications during PS placement. To avoid such perforations, we developed a robotic setup equipped with a multitude of sensors as well as a perforation detection algorithm using the electrical conductivity signal. This method was based on a Bayesian approach, allowing for accurate real-time perforation detection without filtering the signal or prior calibration.

To evaluate the proposed materials and methods, we created a database including 80 drillings in fresh pig lumbar vertebrae. This database contains different types of signals (electrical conductivity, torque, velocity, and position). Numerical and experimental validation on perforation detection was convincing (perforations were avoided in 100% of cases). The results show that electrical conductivity allows the detection of imminent perforations of the spinal canal during actual ex-vivo pedicle drilling. Combined with a robotic drilling setup, this permitted reliably stopping the drilling upon detection in real-time.

Future work will evaluate the method's robustness through in-vivo tests. These will involve a pig whose spine is subjected to physiological motions such as breathing and deformations resulting from the pressure of the drill on the pedicle. The other future task will be to extend the drilling database and make it open-source by including several other signals (position, speed, force, time, video, etc.).

REFERENCES

[1] C. J. Hwang, J.-M. Baik, J. H. Cho, S. J. Yoon, D.-H. Lee, and C. S. Lee, "Posterior correction of adolescent idiopathic scoliosis with high-

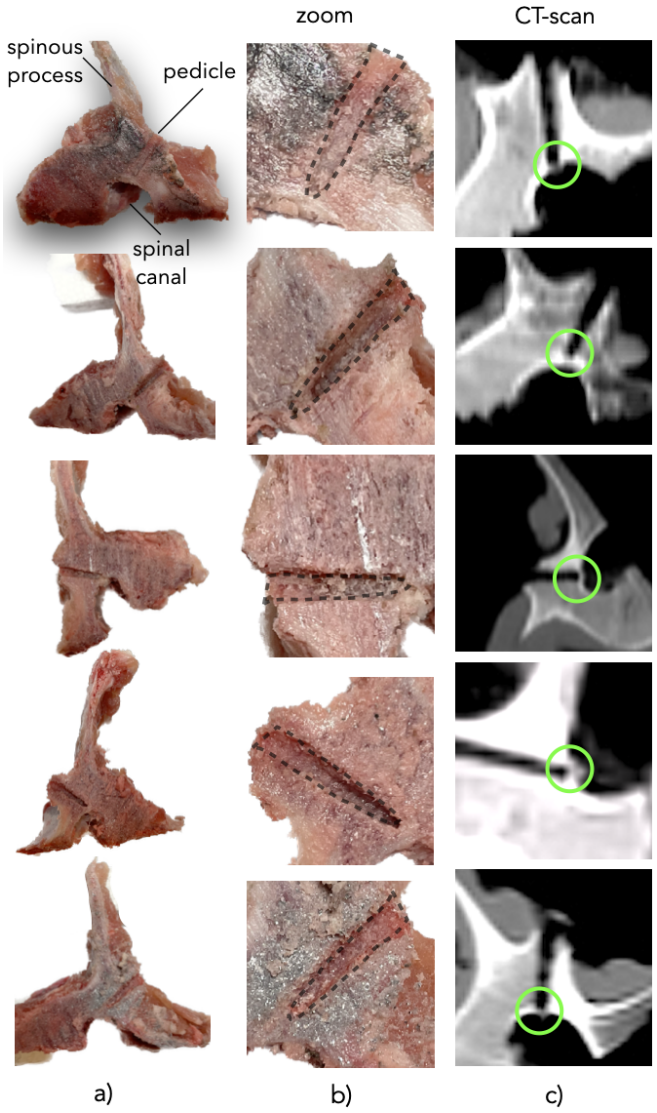

Fig. 10. Sample of 5 (among a total of 24) vertebrae drilled experimentally using the developed robotic set-up and the proposed perforation detection algorithm. a) shows a global view of 5 vertebrae, b) the corresponding zoom on the drilled holes, and c) depicts the CT-scan images of the drilled holes. As can be seen (green circle) the drilling was stopped before the spinal canal, i.e. at the moment of deformation of periostal tissue.

density pedicle screw-only constructs: 5 years of follow-up", *Yonsei Medical Journal*, vol. 61, no. 4, p. 323, 2020.

[2] S. Langensiepen, O. Semler, R. Sobottke, O. Fricke, J. Franklin, E. Schönau, and P. Eysel, "Measuring procedures to determine the cobb angle in idiopathic scoliosis: a systematic review", *European Spine Journal*, vol. 22, no. 11, pp. 2360–2371, 2013.

[3] J. Cobb, *Outline for the Study of Scoliosis*. JW Edwards Publishing Co., 1948, vol. 5.

[4] M. Aebi, "The adult scoliosis," *Euro. Spine J.*, vol. 14, no. 10, pp. 925–948, 2005.

[5] A. C. Koumbourlis, "Scoliosis and the respiratory system", *Paediatric respiratory reviews*, vol. 7, no. 2, pp. 152–160, 2006.

[6] E. Cuartas, A. Rasouli, M. O'Brien, and H. L. Shufflebarger, "Use of all-pedicle-screw constructs in the treatment of adolescent idiopathic scoliosis", *JAAOS-Journal of the American Academy of Orthopaedic Surgeons*, vol. 17, no. 9, pp. 550–561, 2009.

[7] J. N. Weinstein, B. L. Rydevik, and W. Rauschning, "Anatomic and technical considerations of pedicle screw fixation," *Clin. Orthop. and Related Res.*, vol. 284, pp. 34–46, 1992.

[8] A. Faraj and J. Webb, "Early complications of spinal pedicle screw," *Euro. Spine J.*, vol. 6, pp. 324–326, 1997.

[9] J. Tang, Z. Zhu, T. Sui, *et al.*, "Position and complications of pedicle screw insertion with or without image-navigation techniques in the thoracolumbar spine: a meta-analysis of comparative studies," *J. of Biomed. Res.*, vol. 28, no. 3, p. 228, 2014.

[10] M. Farshad, M. Betz, *et al.*, "Accuracy of patient-specific template-guided vs. free-hand fluoroscopically controlled pedicle screw placement in the thoracic and lumbar spine: a randomized cadaveric study," *Euro. Spine J.*, vol. 26, no. 3, pp. 738–749, 2017.

[11] T. Ortmaier, H. Weiß, U. Hagn, *et al.*, "A hands-on-robot for accurate placement of pedicle screws," in *IEEE Int. Conf. on Rob. and Auto.*, 2006, pp. 4179–4186.

[12] J. R. Joseph, B. W. Smith, X. Liu, and P. Park, "Current applications of robotics in spine surgery: a systematic review of the literature," *Neurosurgical Focus*, vol. 42, 2017.

[13] S.-M. Park, H.-J. Kim, S. Y. Lee, *et al.*, "Radiographic and clinical outcomes of robot-assisted posterior pedicle screw fixation: two-year results from a randomized controlled trial," *Yonsei Medical J.*, vol. 59, no. 3, pp. 438–444, 2018.

[14] P. A. Pijpker, J. Kraeima, M. Witjes, *et al.*, "Accuracy of patient-specific 3d-printed drill guides for pedicle and lateral mass screw insertion: an analysis of 76 cervical and thoracic screw trajectories," *Spine*, vol. 46, p. 160, 2021.

[15] W. H. Shuman, A. A. Valliani, E. K. Chapman, *et al.*, "Intraoperative navigation in spine surgery: Effects on complications and reoperations," *World Neurosurgery*, vol. 160, pp. e404–e411, 2022.

[16] O. Suess and M. Schomacher, "Control of pedicle screw placement with an electrical conductivity measurement device: initial evaluation in the thoracic and lumbar spine," *Adv. in Med.*, vol. 2016, 2016.

[17] T. Yurube, Y. Kanda, *et al.*, "Improved accuracy and safety of pedicle screw placement by using a probe with an electrical conductivity-measuring device during severe syndromic and neuromuscular scoliosis spine surgery," *J. of Clin. Med.*, vol. 11, p. 419, 2022.

[18] S. D. Gertzbein *et al.*, "Accuracy of Pedicular Screw Placement In Vivo," *Spine*, vol. 15, no. 1, pp. 11–14, 1990.

[19] P. N. Brett, D. A. Baker, Reyes, *et al.*, "An Automatic Technique for Micro-Drilling a Stapedotomy in the Flexible Stapes Footplate," *J. of Eng. in Med.*, vol. 209, no. 4, pp. 255–262, 1995.

[20] B. Allotta, F. Belmonte, L. Bosio, *et al.*, "Study on a mechatronic tool for drilling in the osteosynthesis of long bones: Tool/bone interaction, modeling and experiments," *Mech.*, vol. 6, pp. 447–459, 1996.

[21] W.-Y. Lee and C.-L. Shih, "Control and breakthrough detection of a three-axis robotic bone drilling system," *Mecha.*, pp. 73–84, 2006.

[22] Y. Hu, H. Jin, L. Zhang, *et al.*, "State Recognition of Pedicle Drilling With Force Sensing in a Robotic Spinal Surgical System," *IEEE/ASME T. on Mech.*, vol. 19, no. 1, pp. 357–365, 2014.

[23] Y.-L. Hsu, S.-T. Lee, *et al.*, "A modular mechatronic system for automatic bone drilling," *Biomed. Eng.: Appl., Basis and Comm.*, vol. 13, pp. 168–174, 2001.

[24] Y. Sun, H. Jin, Y. Hu, *et al.*, "State recognition of bone drilling with audio signal in Robotic Orthopedics Surgery System," in *IEEE/RSJ Int. Conf. on Intel. Rob. and Syst.* 2014, pp. 3503–3508.

[25] J. Da Silva, E. Saghbini, *et al.*, "Automatic bone breach detection for spine surgery based on bio-electrical conductivity sensing: Ex-vivo experimental validation," in *Conf. on New Tech. for Comp. and Rob. Ass. Surg.*, 2022.

[26] R. P. Adams and D. J. C. MacKay, "Bayesian Online Changepoint Detection," *arXiv:0710.3742 [stat]*, 2007.

[27] G. J. J. v. d. Burg and C. K. I. Williams, "An Evaluation of Change Point Detection Algorithms," *arXiv:2003.06222 [cs, stat]*, 2020.

[28] S. Aminikhanghahi and D. J. Cook, "A survey of methods for time series change point detection," *Knowledge and Information Systems*, vol. 51, pp. 339–367, 2017.

[29] K. P. Murphy, "Conjugate Bayesian analysis of the Gaussian distribution," p. 29, 2007.

[30] J. D. Silva, S. Vafadar, T. Chandanson, and G. Morel, "Force control of the KUKA LBR Med without external force sensor," *11 edition of Conference on New Technologies for Computer and Robot Assisted Surgery*, 2022.